Journal of Power Sources 187 (2009) 555–564

Contents lists available at ScienceDirect

Journal of Power Sources

journal homepage: www.elsevier.com/locate/jpowsour

# Study of the Li-insertion/extraction process in $LiFePO_4/FePO_4$

C.V. Ramana[a], A. Mauger[b], F. Gendron[c], C.M. Julien[c], K. Zaghib[d,*]

[a] Department of Metallurgical and Materials Engineering, The University of Texas at El Paso, El Paso, TX 79968, USA
[b] UPMC Université Paris 6, UMR7590, Institut de Minéralogie et Physique de la Matière Condensée, 140 rue de Lourmel, 75015 Paris, France
[c] UPMC Université Paris 6, UMR 7588, Institut des Nano-Sciences de Paris, 140 rue de Lourmel, 75015 Paris, France
[d] Institut de Recherche d'Hydro-Québec, 1800 Boul. Lionel Boulet, Varennes, Que., Canada J3X 1S1

ARTICLE INFO

*Article history:*
Received 11 September 2008
Received in revised form
10 November 2008
Accepted 11 November 2008
Available online 21 November 2008

*Keywords:*
Li-battery
$LiFePO_4$
Cathode
Intercalation
TEM

ABSTRACT

The structural properties of $LiFePO_4$ prepared by the hydrothermal route and chemically delithiated have been studied using analytical electron microscopy and Raman spectroscopy. High-resolution transmission electron microscopy and selected area electron diffraction measurements indicate that the partially delithiated particles include $LiFePO_4$ regions with cross-sections of finite size along the *ac*-plane, as a result of tilt grain boundary in the *bc*-plane, and dislocations in other directions. Only the boundary along the *bc*-plane is accompanied by a disorder over about 2 nm on each side of the boundary. The Raman spectrum shows the existence of both $LiFePO_4$ and $FePO_4$ phases in the shell of the particles at a delithiation degree of 50%, which invalidates the core–shell model. This result also invalidates the recent model according to which each particle would be single-domain, i.e. either a $LiFePO_4$ particle or a $FePO_4$ particle. On the other hand, our results, like prior ones, can be understood within the framework of a model similar to the spinodal decomposition of a two-phase system, which is discussed within the framework of morphogenesis of patterns in systems at equilibrium. Both end-members, however, are well crystallized, suggesting a recovery similar to that observed in superplastic alloys, with dynamics that are due to the motion of nucleation fronts and dislocations, and not due to a diffusion phenomenon associated with a concentration gradient.



## 1. Introduction

$LiFePO_4$ is now recognized as the active cathode element for the new generation of lithium batteries. This material has been known for its low cost, non-toxicity, and remarkable thermal stability for some time [1]. Carbon coating of the particles to overcome their low intrinsic electronic conductivity [2], reduction of the size of the particles [3], and the recent progress to free the material from impurities [4,5] have made possible the preparation of samples with full capacity ($170\,Ah\,kg^{-1}$) at moderate power densities [6], even under tough conditions [7]. Due to the important impact of this material in the construction of Li-batteries for a wide range of applications from portable electronics to hybrid electric vehicles, it is important to understand the fundamental properties of the material, starting with the transport properties which are crucial for the battery industry. Indeed, such investigations have been the subject of many studies and of a debate on the importance of ionic versus electronic conductivity [8–10]. In recent work, we have argued that the intrinsic dc electrical conductivity (less than $10–9\,S\,cm^{-1}$ at room temperature) is not due to the lithium ions as it has been assumed sometimes in the past. Instead, but it is due to the hopping of the d-hole on a $Fe^{3+}$ site that forms a small magnetic polaron [11]. These electrical measurements have then been used to understand the electronic transport, but they give little information on the diffusion of the Li ions.

The diffusion process for the Li ions is still subject to debate. $LiFePO_4$ crystallizes in the olivine structure (space group *Pnma*) shown in Fig. 1. The $FeO_6$ octahedra sharing corners form layers in the *bc* planes. The layers are linked together by $PO_4$ tetrahedral units. The lithium ions are located in the space left by the $PO_4$ units, between the Fe-O layers that are blocking for the Li diffusion. Yet the *b* and *c* directions are not equivalent, and the energy barrier that the Li has to overcome to move from one unit cell to the next one is 0.55 eV along the *b*-direction, compared with 2.89 eV along the *c*-direction [9]. In practice, the Li-ions will move along the path that requires a minimum energy, so that they will "slalom" in the *b*-direction [8]. The motion is then one-dimensional. This information, however, is not sufficient to understand the ionic conductivity in the lithiation/delithiation process, because the motions of neighboring Li ions are correlated. This correlation is best shown by the fact that the solid solution $Li_xFePO_4$ does not exist under "normal" conditions in particles that are large enough so that size effects are negligible. A solid solution exists at high temperature, at any value of $x$ in the range $0 \le x \le 1$ [12–16], but in the range

* Corresponding author. Tel.: +1 450 652 8019; fax: +1 450 652 8424.
*E-mail address:* zaghib.karim@ireq.ca (K. Zaghib).

0378-7753/$ – see front matter © 2008 Elsevier B.V. All rights reserved.
doi:10.1016/j.jpowsour.2008.11.042

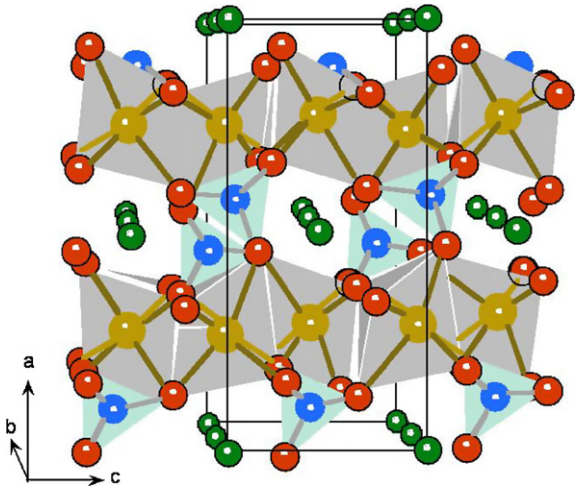


**Fig. 1.** Representation of the olivine-like structure of $LiFePO_4$. The $FeO_6$ octahedra sharing corner form layers in the *bc* plane. The layers are linked together with $PO_4$ tetrahedral units.

of temperature ($T \leq 60\,^{\circ}C$) explored in the present work, there is a miscibility gap between $FePO_4$ and $LiFePO_4$, except close to the end-compositions. The detection of the intermediate phases above the critical temperature implies that the single-phase region might be modified under some conditions. In particular, Richardson has recently reported that upon heating at 375 °C, then cooling in different steps, with each step held for 2 h, it is possible to obtain samples that are a mixture of the end-members plus the $Li_{0.60}FePO_4$ and $Li_{0.34}FePO_4$ homogeneous solutions [17]. But unless such a particular heat treatment is performed, a rapid de-mixing occurs upon cooling, and we are left with two phases, namely $Li_{1-\alpha}FePO_4$ and $Li_\beta FePO_4$, where $\alpha$, $\beta$ denote the width of the single-phase regions [18]. Yet, these parameters are small for large particles, say for particles of diameter $d \geq 45$ nm, so that to a first approximation, the lithiation/delithiation process involves $xLiFePO_4 + (1-x)FePO_4$ and not $Li_xFePO_4$ solid solutions. The miscibility gap decreases upon decreasing the size of the particles below 100 nm, so that the solid solution should be stabilized below a critical size that is smaller than 45 nm [19]. This has recently been confirmed by the observation of a solid solution in 40 nm-sized particles [20]. In the present work, we deal with particles of size ≈100 nm for which such size effects are still negligible, so that the two phases are not soluble.

This insolubility is of basic importance on the dynamics of the extraction or insertion of lithium. In the classical situation of a single phase, it would have been possible to define a diffusion coefficient $D$, from Fick's law that relates the diffusive current $\vec{j}$ to a concentration gradient $\vec{j}_d = -D\overrightarrow{grad}(x)$. At equilibrium, this current is compensated by the current $\vec{j}_f = x\vec{F}$ induced by a driving force $\vec{F}$ due to the electric field. At equilibrium, where the distribution of the moving species satisfies the Maxwell–Boltzman distribution, the equation $\vec{j}_d + \vec{j}_f = 0$ leads to the Nernst–Einstein law $v = DF/(k_BT)$ with $v$ as the drift velocity. This law has been used to estimate the diffusion coefficient in the past, either by assuming that $v$ can be deduced from electrical conductivity measurements [21] (but we have already shown that this is not justified, since it is a measure of the electronic conductivity), or by measurements taken from cyclic voltammograms [22–25]. This last approach via electrochemical properties may be more reliable, since they are directly related to $Li^+$ insertion/extraction. But still, such estimates are based on two assumptions. One is the hypothesis that thermodynamic equilibrium is achieved, and we have previously argued that the Nernst–Einstein relation is strongly violated in out-of-equilibrium systems [26]. As we shall see, however, this hypothesis is reasonable. The other hypothesis is the existence of a diffusion process for Li-ions, associated to a gradient of concentration in a crystalline solid solution, and the separation in two phases $LiFePO_4$–$FePO_4$ makes it questionable [25]. The width of the boundary between the two phases is about 4 nm [27], i.e. large enough to allow some concentration gradient associated with the structural disorder within [28]. Nevertheless, it is possible that the lithium extraction/insertion occurs via the motion of a nucleation front, the kinetics of which is of a different nature [27]. Some recent work even suggests that the $FePO_4/LiFePO_4$ interface is the juxtaposition of the two end-members and not a solid solution [29], which requires that the lithium extraction/insertion occurs via the motion of a nucleation front. In any case, the collective and thus highly correlated Li-motion implies that general diffusion laws are not relevant to describe the motion of lithium on the atomic scale. In the present work, we still use the diffusion equation to describe the dynamics of the Li-motion, but on the scale of the characteristic length $\lambda$ of the spinodal decomposition. In addition, this diffusion equation is just used as a convenience to illustrate this effect, which can occur irrespective of the nature of the kinetic equation, whether it is of a diffusive type or not.

The symmetry of the lattice and the preferential diffusion of Li along the *b*-direction is not sufficient to determine the geometry of the interface between $FePO_4$ and $LiFePO_4$, which can lie, according to different reports, in the (*bc*) plane [27] or in the plane ([1 1 0], *c*) [29]. Different studies are promoting the displacement of the interface to model the Li insertion/extraction process [1,27–30]. These models, however, are not equivalent. The first one is the so-called "core–shell" model, according to which the interface separates a $LiFePO_4$ core region from a $FePO_4$ shell [1] during both the charge and discharge process. An extension of this model has this scenario during the charge process, while assuming the opposite holds true during discharge from the fully charged state $FePO_4$, namely a $FePO_4$ core region surrounded by a $LiFePO_4$ shell [25] (again, we present here a simplified version of the model by taking $\alpha = \beta = 0$). Recent electron microscopy studies, however, have shown this model does not work, since Li extraction leads to the formation of $FePO_4$ domains [27]. The mosaic model [31] takes into account the possibility of the extraction/insertion of lithium to start at different nucleation sites. The question as to whether these nucleation sites are located at several points on the crystal surface [27] or are more distributed below the surface is still unknown. In particular, the HRTEM images in [27] correspond to a situation where dislocation lines parallel to the *c*-axis, generated by the lattice mismatch between $LiFePO_4$ and $FePO_4$, have already nucleated into an extended phase boundary. The topology of the domains depends not only of the models, but also of the samples: in some cases, we have the images of stripes [27] with (*bc*) interfaces [27], or shells [29].

Yet the common feature between the different models is that they assume the existence of an interface, i.e. the coexistence of $LiFePO_4$ and $FePO_4$ regions inside each particle. This is now challenged by a new model [32], according to which the lithiation/delithiation of each particle would be so fast (domino-cascade model) that the particles should be either totally charged or totally discharged. In this scheme, at degree of delithiation $x$ so that the overall composition of the powder is $xLiFePO_4 + (1-x)FePO_4$ (usually written $Li_xFePO_4$ in the literature to make it shorter, not to be confused, however, with the chemical formula of a solution), the powder would be made of a fraction $x$ of $LiFePO_4$ particles and a fraction $(1-x)$ of $FePO_4$ particles.

In this context, we found it to be desirable to pursue the investigation to test these different models, aiming at a better understanding of the efficiency of this material as a cathode. In this work, we report HRTEM experiments on $LiFePO_4$ particles (average size 100 nm) before and after delithiation, and also at an intermediate delithiation degree ($x = 0.5$). Raman spectroscopy

measurements have also been done to characterize the surface layer. In the partially delithiated sample, we find the existence of $LiFePO_4$ domains. One of the interfaces is along the *c*-axis in the (*bc*) planes, in agreement with Refs. [27,29], confirming the insertion/extraction process of these prior works. On another hand, our results are compatible neither with the core–shell model, nor with the "domino-cascade model". We find that defects such as a grain boundary favor the formation of $LiFePO_4$ domains during the partial extraction of lithium, and the lattice distortion associated with the lattice mismatch between the two phases is accommodated by the formation of dislocations, some of them parallel to the *c*-direction, in agreement with prior work. However, we also observe other interfaces along [1 0 1] and *a*-directions, allowing for the cross-section of the $LiFePO_4$ domains in the (*ac*) planes to be of finite size. Both end-members, however, are well crystallized, a result we discuss as an example of extended recovery similar to the one observed in super-plastic alloys compounds.

## 2. Experiments

### 2.1. Synthesis

$LiFePO_4$ specimens were prepared in a laboratory Teflon-lined autoclave by the hydrothermal route pioneered by Zaghib and Armand [33], also reported in subsequent publications [34]. The stoichiometric amount of the precursors, jet-milled iron oxalate, $H_3PO_4$ and LiOH were thoroughly mixed together. The autoclave was filled with distilled water and maintained at 165 °C for 4 h, and then cooled down to room temperature. Carbon-coated $LiFePO_4$ grown by the cellulose route was prepared from solution in acetone [4]. The initial quantity of cellulose acetate (5 wt.%) corresponds to ca. 1.2 wt.% of carbon in coated $LiFePO_4$ samples. After drying, the mixture was heated at 700 °C for 2 h under argon flow. Note that the choice of this moderate sintering temperature minimizes the amount of $Fe^{3+}$ions in the powder, and the absence of any impurity phase has been checked by magnetic measurements of both magnetization curves and magnetic susceptibility.

The $LiFePO_4$ materials were delithiated chemically by the use of potassium persulfate ($K_2S_2O_8$) in an aqueous solution. The molar ratios of $LiFePO_4$:$K_2S_2O_8$ were 4:1 and 2:1 for the $x = 0.5$ and 0.0 samples, respectively. The mixture $LiFePO_4$ and $K_2S_2O_8$ dissolved in water was stirred at room temperature for 24 h. The powders were washed, filtered and dried at 80 °C. The *x*(Li) was verified by inductively coupled plasma spectrometry (ICP) and X-ray diffraction (XRD) measurements. Both methods gave the same values.

### 2.2. Characterization

Transmission Electron Microscopy (TEM) analysis has been performed using a JEOL TEM2010F at a 200 kV acceleration voltage. Phase and structure of the material have been monitored using selected area electron diffraction (SAED). For TEM analysis, the powder sample was dispersed on a 3-mm Cu-grid with a hole size of 1 mm × 2 mm. High-resolution transmission electron microscopy (HRTEM) imaging along with SAED measurements were performed as a function of *x* in $Li_xFePO_4$. Fast Fourier transformation (FFT) was carried out by Gatan Digital Micrograph 3.4.

XRD patterns were obtained using a Philips X'Pert PRO MRD (PW3050) diffractometer equipped with a Cu anticathode (Cu Kα radiation $\lambda = 1.54056$ Å) at room temperature. The measurements have been recorded under Bragg–Brentano geometry at $2\theta$ with a step of 0.05° in the range 10–90°.

Raman spectra were recorded on a Jobin-Yvon U1000 double monochromator using the 514.5-nm line from a Spectra-Physics 2020 argon-ion laser. Standard photon-counting techniques were used for detection. In a typical spectral acquisition, six Raman scattering spectra, each recorded with a resolution of 2 $cm^{-1}$, were averaged. Care was taken against sample photodecomposition using a low excitation power of 10 mW.

The electrochemical properties were measured in cells with metallic lithium as the negative electrode. The electrode was 1 M $LiPF_6$ in ethylene carbonate (EC) + diethyl carbonate (DEC).

## 3. Results

### 3.1. X-ray and electron microscopy

The XRD patterns of the samples are shown in Fig. 2. All the diffraction lines can be indexed in the orthorhombic system with the *Pnma* space group. The refined lattice parameters of $LiFePO_4$ are $a = 10.3298(2)$ Å, $b = 6.0097(8)$ Å, $c = 4.693(1)$ Å, and $V = 291.3(3)$ $Å^3$, all of which are in good agreement with the literature values [12,13,35,36]. The average mono-crystallite size was calculated from the XRD line width using Scherrer's formula, $d = 0.9\lambda/\beta_{1/2}\cos\theta$, where λ is the X-ray wavelength, $\beta_{1/2}$ is the corrected width at half-height of the main diffraction peaks, and $\theta$ is the diffraction angle. The procedure to determine $\beta_{1/2}$ has been reported elsewhere [37]. The parameter *d* has been measured for different angles corresponding to the (2 0 0), (1 0 1), (1 1 1), (2 1 1) and (3 1 1) lines. No significant dependence on $\theta$ was evident, and the result is $d = 37 \pm 5$ nm. The XRD pattern on the $x = 0.5$ sample is the superposition of both end-members, as expected for a two-phase system, but the lines are slightly shifted with respect to the end-members. The shift in $2\theta$ for the [3 1 1] line for instance, is 0.03° for $LiFePO_4$, and rises to 0.1° for $FePO_4$. These shifts are in agreement with prior results reported in Ref. [18] and correspond to the fact that the two-phase system is a mixture of $Li_{1-\alpha}FePO_4$ and $Li_\beta FePO_4$, as mentioned in Section 1. For $Li_\beta FePO_4$, the lattice parameters are $a = 9.775$ Å, $b = 6.000$ Å and $c = 4.75$ Å. Rietveld refinement confirms the state of charge $x = 0.50 \pm 0.01$. From now on, in order to simplify notations we use the same notation LFP to denote either the $LiFePO_4$ phase (fully discharged state) or the $Li_{1-\alpha}FePO_4$ (Li-rich phase in partially discharged particles). In the same way, we use the same notation FP for the $FePO_4$ phase (fully charged state) and $Li_\beta FePO_4$ (Li-poor phase in partially discharged particles). The average coherence length *d* is also independent of the degree of delithiation *x*, in agreement with the results reported for this material [32]. In addition, the magnetic measurements, which are a much more sensitive way to check the presence of impurities [38], show that the magnetization is linear with field up to 30 kOe at any temperature $T \geq 4$ K, and the samples are free of any impurity.

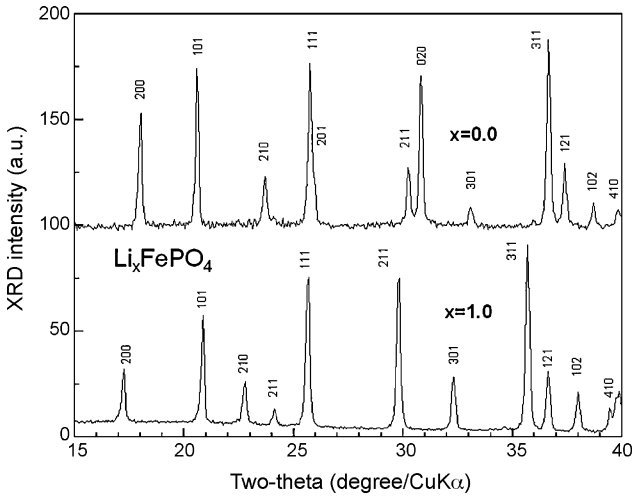


**Fig. 2.** XRD patterns of $LiFePO_4$ and $FePO_4$. Both diagrams were indexed in the orthorhombic (*Pnma*) crystallographic system.

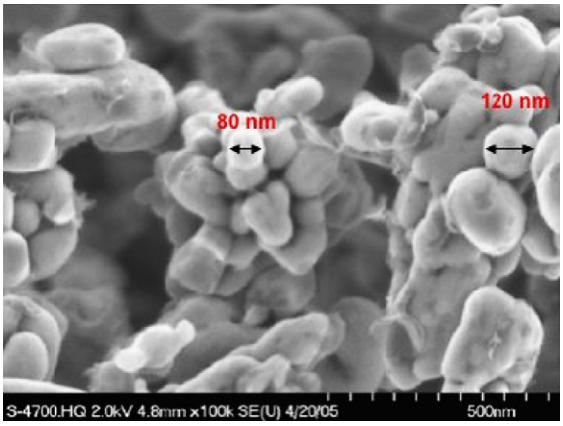


**Fig. 3.** SEM image of the pristine $LiFePO_4$ powders synthesized by the hydrothermal route, followed by carbon coating.

The SEM images (Fig. 3) show that the particles have a more spherical shape than those investigated in Ref. [27]. However, the particles are faceted, as in Ref. [27], as expected from their simulated morphology, according to which the large faces lie in the (*ac*)-plane, with the long axis parallel to *c* [39], in agreement with the identification of these phases from the TEM. The average size of the primary particles was 100 nm.

The TEM data, which include the selected area electron diffraction patterns (SAED) and the high-resolution lattice images (HRTEM) of the samples investigated in this work, are shown in Figs. 4–6. The HRTEM and SAED patterns of the end-members LFP and FP in Figs. 4 and 5 provide evidence for the structural quality of the samples examined. The bright-field, low-magnification TEM images of the samples (not shown) indicate that the material contains spherically shaped crystallites as confirmed by the SEM and XRD measurements. We first focus attention on the data of LFP (Fig. 4). The inset (Fig. 4A) shows the Fast-Fourier-Transform of the HRTEM image, which indicates the direction in which the crystallite was examined and lattice planes contributing to the diffraction. The ordered lattice fringes in the HRTEM obtained along the [0 $\bar{1}$ 0] zone-axis are due to the crystalline nature of the LFP sample. The SAED pattern (Fig. 4B), which was obtained in the same position as in HRTEM, i.e. along the [0 $\bar{1}$ 0] zone axis, indicates the diffraction maxima due to reflections from the (1 0 0) and (0 0 1) lattice planes of LFP. The measured fringe spacing values are 1.032 nm and 0.467 nm in the vertical and horizontal directions, respectively, as indicated in Fig. 4A. We now turn to the electron microscopy data of the FP sample (Fig. 5). The ordered lattice fringes (Fig. 5A) in HRTEM and diffraction maxima in SAED (Fig. 5B) (both of these are obtained along the same [0 $\bar{1}$ 0] zone axis) are evident for the FP sample. The lattice fringe spacing values obtained are indicated in Fig. 5. Similar arguments, as made for LFP, can be made for the structural quality of the FP sample without further explanation since the data were obtained in the same zone axis as for LFP.

The most interesting part of the electron microscopy analysis work comes from the data of the $x = 0.5$ sample. The HRTEM image is shown in Fig. 6. This image shows an LFP domain (the part with lighter contrast) in an FP region. The FFTs obtained from the LFP and FP domains are shown as inserts in Fig. 6. The area of lighter contrast in the HRTEM image is used to obtain the FFT of the LFP domain whereas the FFT of the FP domain is taken from the dark region just above the LFP domain. A couple of FFTs taken across the boundary, separating the LFP and FP domains for which the FFTs are shown, are also displayed as inserts (labeled as B representing the boundary). These FFTs, taken in a small region across the boundary of the LFP and FP phases with different lattice parameters, provide important information. The LFP and FP phases are

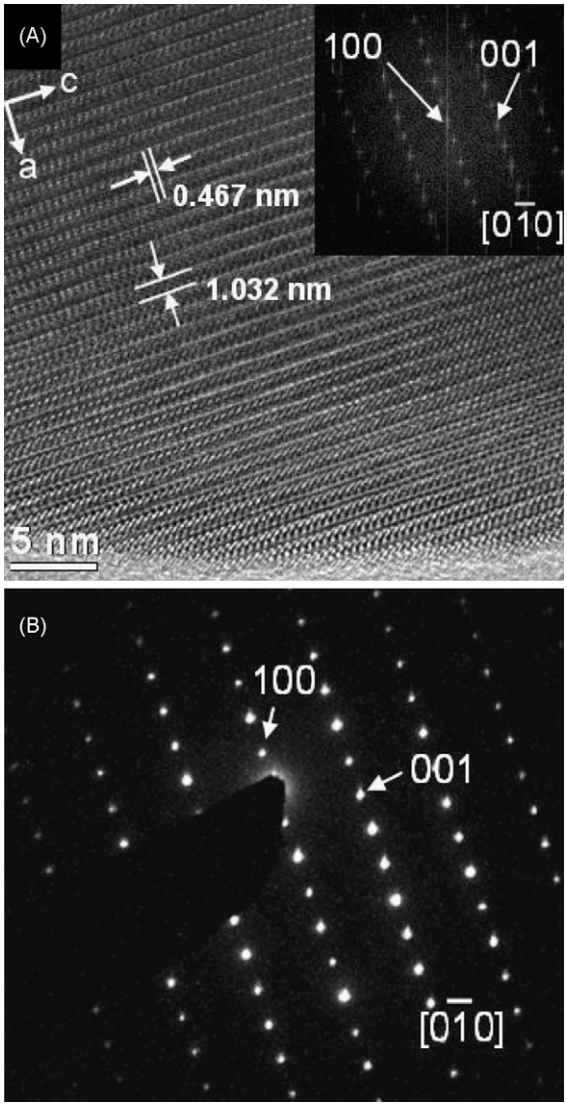


**Fig. 4.** (A) HRTEM images of $LiFePO_4$ obtained by hydrothermal process. The zone axis is [0 $\bar{1}$ 0]. The FFT of the image is shown in insert. (B) SAED patterns of $LiFePO_4$, obtained along the same zone axis. The assignment of diffraction maxima and the direction of view are indicated.

compositionally different and exhibit a lattice parameter difference of approximately 0.5 Å (10.32 Å *vs.* 9.77 Å) along the *a*-axis. Therefore, although this is a small difference, a broadening or splitting of the maxima of the reflections, compared to the sharp reflections in the individual phases, along the *a*-axis can be expected since the electron diffraction probe is much more sensitive to the local structure as compared to the X-ray diffraction. This would also provide an argument against the validity of the two-phase system and not due to an island caused by a defect in the same phase. As such, the FFT of the boundary is taken to visualize this effect in the present case. As evident in the FFTs of the boundary in Fig. 6, streaking and spot-broadening due to the overlap of two reflections is clearly observed along the direction of *a*-axis as indicated by the arrows. This provides clear evidence and/or a direct confirmation of the fact that it concerns the two LFP and FP phases, which are compositionally different with different lattice parameters. Having established that it concerns the LFP domain in a region of the FP domain, we now focus our attention to further explain the mechanism involved. One boundary of the LFP domain is parallel to the *c*-direction. This is outlined as a broken line in the picture. This is the typical boundary line that was evident from Ref. [27]. In this prior work, however, the

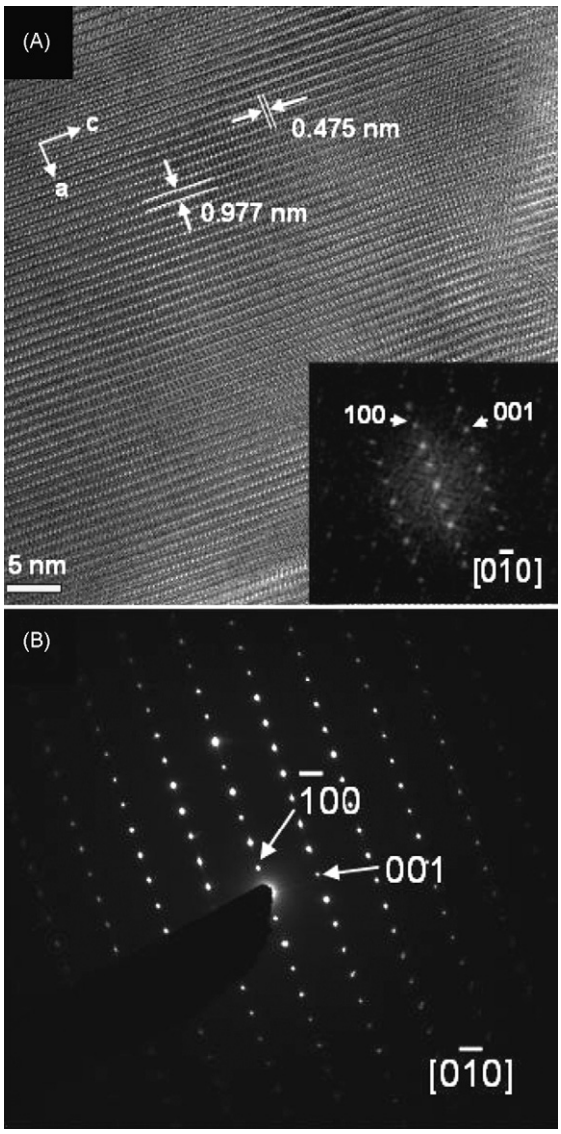


**Fig. 5.** (A) HRTEM images of $FePO_4$ obtained by chemical delithiation of the $LiFePO_4$ sample prepared by hydrothermal process. The FFT of the image is shown in insert. (B) The corresponding SAED pattern of the sample. Both the HRTEM and SAED patterns are obtained along the [0 $\bar{1}$ 0] zone axis.

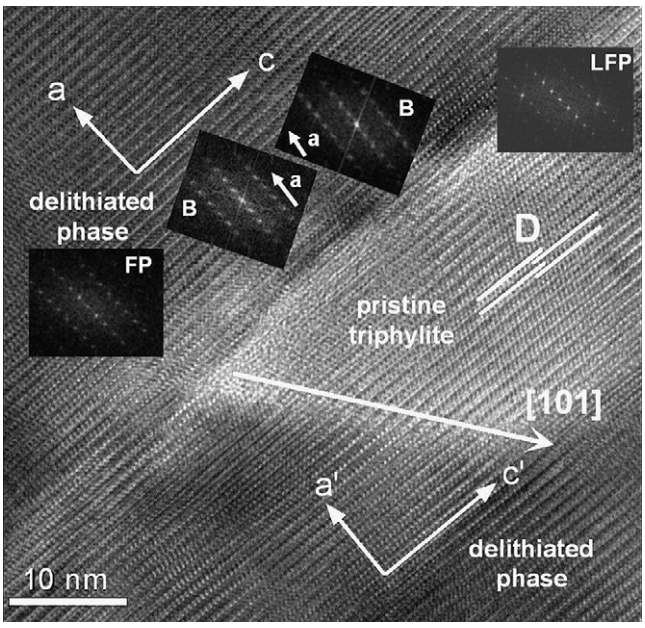


**Fig. 6.** HRTEM image of the $0.5(LiFePO_4 + FePO_4)$ sample showing a $LiFePO_4$ cluster in the *ac*-plane. A tilt grain boundary with an angle $\theta = 3.3^\circ$ is observed at the interface along the *c*-direction. The *a*- and *c*-direction, and the same directions rotated by $\theta = 3.3^\circ$, referred as *a*′, *c*′ are shown on both sides of the grain boundary, in the regions where these orientations are observed. One another edge of the $LiFePO_4$ cluster is along the (1 0 1) direction and is visualized by an arrow. The other boundary is along the *a*-direction with dislocation line marked in the "D" region by straight lines along atomic layers on both sides. Inserts are the FFT of the selected regions, namely $LiFePO_4$ (LFP) domain, $FePO_4$ (FP) domain and across the boundary (B). The splitting of spots of diffraction maxima along *a*-direction due to a compositional difference along with lattice parameters (see text) is evident in the FFTs represented as "B" (for boundary).

TEM experiments essentially showed a continuous boundary line extending up to the surface of the sample. The situation in Fig. 6 of the present work shows a more complex situation, where the cross-section of the LFP domains in the (*ac*) planes are of finite size, although they are distributed along this boundary. Part of the reason why this boundary is parallel to the *c*-direction is linked to the topology of the lattice, since the material can be viewed as a piling of dense atomic (*bc*)-planes formed by the $FeO_6$ octahedra sharing corners (separated by $PO_4$ units). This situation favors the formation of structural defects along the *c*-axis to accommodate the lattice distortion due to the migration of $Li^+$ along the *b*-direction. The boundary of the LFP domain along the *c*-direction is then confirmation of the model in Ref. [27], according to which the formation of FP generates strong stress fields in the (*ac*)-planes. The phase boundary is viewed in [27] as the nucleation of dislocation lines parallel to the *c*-axis. The present work, however, shows that the LFP domains are distributed along this same line along the *c*-direction, which suggests that this line in Fig. 6 is just the projection in the *ac*-plane of a structural defect in the *bc*-plane, namely a tilt grain boundary of tilt angle 3.3°. This is best shown in Fig. 6, where we have drawn the directions of the *a*- and *c*-axis on both sides of the boundary. This phenomenon seems to be quite a basic property of the material, since Chen et al. have also noticed in their work [27] that, although the reaction is topotactic, a slight rotation between the two phases is generally observed. Our result, however, shows that this rotation is not restricted to the boundary between the two phases, since the cross-section of the LFP domains are of finite size in the (*ac*) plane, while the tilt extends at a larger length scale. The picture is then that of a tilt grain boundary that has been formed upon the strains and lattice deformations formed in the delithiation process. The pre-existence of such a grain boundary in the homogenous LFP is unlikely, since the tilt angle is very small and is not related to any natural topological angle associated to the geometry of the olivine structure, and indeed, we did not observe it (see Fig. 4). On the other hand, we did not observe such a tilt after complete delithiation either (see Fig. 5). The evolution of these structural defects upon the insertion/extraction process might then be similar to the so-called continuous recrystallization process (CRP) of some superplastic aluminum alloys [40], except that the CRP is driven by the thermal fluctuations, while here, it is assisted by the lithiation/delithiation process that generates a strain flow. If the term CRP is reserved for the case where the migration of high-angle grain boundaries is the driving force, the more correct term "extended recovery" should be used (for further discussion, see Ref. [40], since no large angle grain boundaries have been detected). The role played by the grain boundaries in superplastic alloys is also played by the FP/LFP interface in our material. Yet the microstructural processes responsible for such a recovery are not completely understood, but some arguments have been invoked. In particular, the disorientation is related to the migration distance because it relieves the lattice curvature introduced by rolling. Nes [41] proposed that an increase in

grain boundary disorientation was attributable to the fine particles dissolving ahead of migrating grain boundaries, an effect termed "strain-induced particle reversion". In the same way, the existence of the tilt grain could be due to the formation of FP or LFP domains (that have about the same size as the fine particles in the superplastic alloys). The main difference is that the particles reform immediately after the grain boundary progresses in superplastic alloys, while in the present case the "particle" is not reformed, as it has disappeared owing to the extraction/insertion process that has modified the strain fields. As in the superplastic alloys, we can envision a recovery that involves low-angle grain boundaries [42], continuity between the sliding boundaries being achieved by the generation, migration and absorption of dislocations.

The boundary along the *c*-direction shows some disorder, so the width of this perturbed region extends over about 4 nm, but only in the interfacial region between LFP and FP. Yet, even this interface region is not amorphous, in agreement with Ref. [27]. In addition, we find here that there are other interfaces evident in Fig. 6 along the (1 0 1) direction, and also along the *a*-direction. Along these two directions, the strains result in the formation of dislocations. This is shown in the figure by the straight lines we have drawn to visualize the (*bc*) atomic planes that are shifted on both sides of the line defects. However, the lattice on both sides of these lines is well organized, in contrast to the interface along the *c*-direction. The interface in the [1 0 1] direction is sharp, like the interface in the ([1 1 0], *c*) plane envisioned in [29]. These additional interfaces are responsible for keeping finite the size of the cross-section of the domain in the (*ac*)-plane. It does not reveal anything about the size of the domains along the *b*-direction.

### 3.2. Raman spectroscopy

The penetration depth of the laser light used in Raman spectroscopy is a few nanometers. For this reason, Raman spectroscopy has been extensively used to characterize the carbon deposit on the particles used in Li-batteries [43]. For the same reason, Raman spectroscopy has been the only technique able to detect the presence of lithium hydroxide and lithium carbonate on the surface of the particles exposed to moisture [44]. In the present case, we used it to determine the LFP/FP ratio in the vicinity of the surface. In a core–shell model, at a stage of delithiation $x = 0.5$, the shell probed by Raman spectroscopy should be FP only.

The Raman spectra of both end-members LFP and FP have been studied in Refs. [45,46], respectively. The Raman spectrum of our $x = 0.5$ sample is reported in Fig. 7, together with that of the same LFP sample before delithiation. For clarity, vertical broken lines have been added to mark the Raman lines of LFP published in [45] together with their assignment. The Raman spectrum of FP is mainly characterized by lines marked in Fig. 7. They have been selected because they are located at wavenumbers where there are no Raman lines of LFP in their vicinity. Those are the two lines at 306 and 338 $cm^{-1}$, both located in the gap between the *T*-vibration mode at 238 $cm^{-1}$ and the $\nu_2$ mode at 442 $cm^{-1}$ of LFP, and the line at 911 $cm^{-1}$ in the spectral gap between the $A_g(\nu_4)$ and the $A_g(\nu_1)$ mode of LFP. Therefore, we find that the Raman spectra of the $x = 0.5$ sample is just the superimposition of the Raman spectra of the two end-members. The same result has been observed previously for the $x = 0.11$ sample, and shows that the region probed by the Raman spectroscopy, i.e. the few-nanometer thick shell of the particles, is a two-phase system [47]. The LFP/FP ratio can be deduced from the relative intensity of the lines with respect to pure LFP and FP samples, which invalidates the core–shell model, and corroborates the idea of the mosaic model, according to which the Li-insertion/extraction occurs from many nucleation sites at the surface so that both phases co-exist in the shell. It does not mean, however, that the particle is homogenous at a mesoscopic scale,

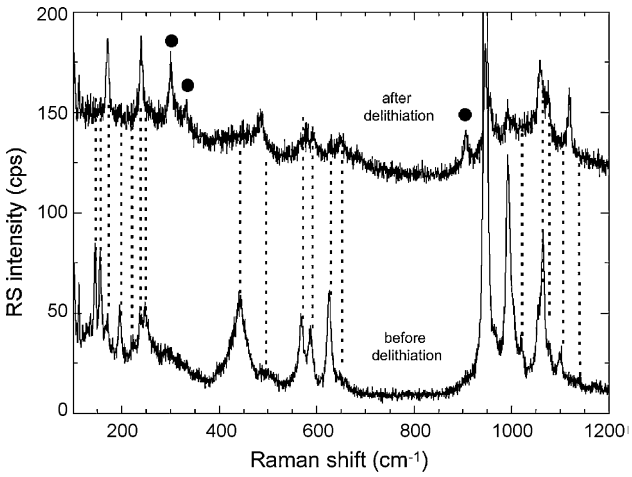


**Fig. 7.** Raman scattering spectra of $LiFePO_4$ and the chemically delithiated phase $0.5(LiFePO_4 + FePO_4)$. Dashed lines have been drawn to point to Raman peaks characteristics of the $LiFePO_4$ phase. The dots point to the peaks characteristics of the $FePO_4$ phase.

i.e. that the LFP/FP ratio is the same in the shell and in the core region. In particular, the shell composition cannot be determined from the ratio of the intensities of Raman lines associated with the end-members, because the absorption of the particles varies with the composition. However, the Raman spectrum shows that the surface region, just like the core region, is bi-phased.

### 3.3. Electrochemical performance in relation to the structural properties

Fig. 8 presents the electrochemical performance of C-$LiFePO_4$/$LiPF_6$-EC-DEC/Li cells at 60 °C. The charge-discharge curves were obtained by cycling at the C/4 rate in the voltage range 2.2–4.0 V versus $Li^0/Li^+$.

The voltage versus capacity curve gives evidence of the broad plateau that is unanimously reported in all the prior studies (except when dealing with very small particles, in which case the solid solution is stabilized, as already mentioned). This plateau at $V = 3.4$ V is understood to be the signature of the coexistence of both phases inside the particles. This is fully consistent with the observation of these two phases in the HRTEM experiments, but again it is not consistent with the claim in Ref. [32] that the particles are single-

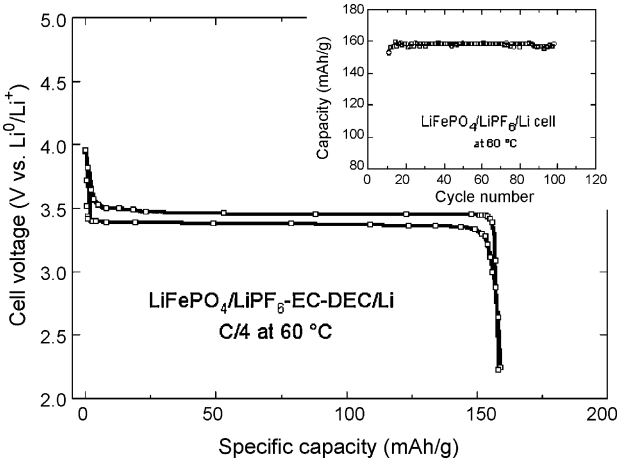


**Fig. 8.** Electrochemical performance of the C-$LiFePO_4$/$LiPF_6$-EC-DEC/Li cells at 60 °C after 100 cycles. In insert is reported the specific capacity as a function of the cycle life under the same conditions (C/4, 60 °C).

phased. To be more specific, the Gibbs' phase rule states that the relation among the number of degrees of freedom $f$, the number of independent components $c$, in a closed system at equilibrium is given by $f = c - p + n$, with $n$ the number of the intensive variables necessary to describe the system, except the mole fractions of the components in each phase. In electrochemical studies, the intensive quantities are only temperature and pressure, but they are kept constant, so that $n = 0$. Here, we deal with a binary system ($c = 2$), consisting of the LFP and the FP phase. If only one phase exists in a particle, $p = 1$ and $f = 1$ so that the potential is a degree of freedom and varies with the lithium concentration. On another hand, if the particles contain the two phases, $p = 2$, so that $f = 0$, in which case no intensive variable (e.g. potential) can change). Therefore, the model of Ref. [32] according to which there is only one phase inside each single (isolated) particle while the electrochemical properties show the characteristic voltage plateau violates Gibbs' rule. Note we have discussed the existence of the plateau in terms of the Gibbs phase rule, which is the original thermodynamic approach in Ref. [1]. It can also be discussed in terms of the minimum of the Gibbs energy to equilibrate the chemical potential between the two phases, which is an equivalent thermodynamic approach [48].

The inductive effect due to the transmission of the electronic charge (the $t_{2g}\downarrow$ electron on the d-shell of $Fe^{2+}$) through the Fe–O–P chain at atoms is important [49,50]. The strong P–O covalence stabilizes the anti-bonding $Fe^{3+}/Fe^{2+}$ state through this Fe–O–P inductive effect. That is why LFP has a high lithium intercalation voltage of 3.4 V versus lithium metal. Therefore, the high value of the potential of the plateau is the proof that the transfer of charge on iron associated to the lithium extraction occurs through this atomic chain involving the phosphate units. Again, this can be done only at an interface inside the particles, which opposes the domino-cascade model after which such an interface would not exist in particles that would be in a single phase.

The other lesson we can learn from the insert of Fig. 8 is that the capacity is 160 mAh $g^{-1}$, which is close to its theoretical value, and remains a constant after 100 cycles. The HRTEM experiments show the extended defects generated during the insertion/extraction process to accommodate the strain field due to the difference in the lattice parameters between the two phases are cured at the end of the process (see Figs. 4 and 5). This feature suggests a recovery upon "re-crystallization" similar to the one observed in superplastic aluminum alloys, even if some cracks remain after a much larger number of cycles [51]. The tilt angle grain boundaries in the ($bc$)-planes, a general property of this material since it has been observed on samples with different modes of preparation and particles of different geometries, plays an important role in this 'extended recovery' process. Owing to the tendency of the system to minimize its total energy, the anisotropy of the grain boundary energy with respect to its orientation results in a flat-faceted boundary shape for the case of grain boundaries with small tilt angle. This has been repeatedly observed for such grain boundaries with disorientations close to low $\Sigma$ coincidence site lattice orientation relationship [52–56]. This is also the reason why this boundary in the ($bc$)-plane is found to be flat in our system. In addition, such boundaries are known to remain straight, i.e. they are displaced parallel to themselves, in contrast to the case of grain boundaries with larger tilt angles for which the motion is accompanied by a permanent shape change (bending and multifaceting). For the case of the aluminum alloy as above-mentioned, the critical disorientation angle that separates the two types of grain boundaries is $\approx 12^\circ$ [57]. The tilt angle in our material is only $3.3^\circ$ and clearly corresponds to the case of grain boundaries that shift parallel to their position. Such a motion of the grain boundary, however, implies the cooperative motion of the lithium ions in the different $b$-channels along the grain boundary. This is confirmation of the lithiation/delithiation process envisioned in [27], and the reason why the lithiation/delithiation process in LFP/FP is so efficient.

## 4. Analysis and morphogenesis

The de-mixing in domains upon lithiation/delithiation is actually quite similar to spinodal decomposition [58]. In this context, for a mixture of A- and B-type materials, the Landau free energy:

$$F = \int dx \left( \frac{A}{2}\Phi^2 + \frac{B}{4}\Phi^4 + \frac{\kappa}{2}(\text{grad}\,\Phi)^2 \right)$$

is a good approximation. $\Phi = \rho_A - \rho_B$ is the density difference of the mixture components. The parameters $A$ and $B$ in the Landau equation are the control parameters that determine the stability of the mixture, and the interfacial energy cost is determined by $\kappa$. The chemical potential is

$$\mu = \frac{\partial F}{\partial \Phi} = A\Phi + B\Phi^3 - \kappa\Delta\Phi$$

where $\Delta$ is the Laplacian operator. If $A < 0$, small fluctuations around $\Phi = 0$ will grow rather than shrink. Often the phase separation occurs via nucleation during the lithiation/delithiation process, as in our case, making the spinodal decomposition difficult to observe. However, if the material has so few defects that the nucleation centers are missing, such decomposition can be observed, as in [27]. Diffusive motion dominates at the length scale of the spinodal decomposition, and the dynamics are governed by the equation of diffusion, which, after linearization around $\Phi_{in}$ (the value of $\Phi$ where the free energy goes through an extremum), and Fourier transform, takes the form:

$$\partial_t \Phi_k(k,t) = -m[(A + 3B{\Phi_{in}}^2)k^2 + \kappa k^4]\Phi_k(k,t) = R(k,t)\Phi_k(k,t).$$

$m$ is the diffusive mobility. The solution has an exponential growth solution with the fastest growing wavenumber:

$$k_{sp} = \left[ \frac{-(A + 3B{\Phi_{in}}^2)}{2\kappa} \right]$$

that quickly dominates the morphology. Therefore, the decomposition results in domains of characteristic length scale $\lambda = (2\pi)/k_{sp}$. When the interface is not flat, the modulation parameter $\lambda$ is simply the typical width of wrinkles that form a labyrinthine pattern. In the present case, however, where the interfaces remain flat, the structure takes the form of periodic stripes in the ($bc$) plane, with $\lambda$ the lamellar spacing, well observed in Fig. 3 of Ref. [27]. This figure shows that $\lambda \approx 50$ nm, which is also the order of magnitude of the domains in our material, except that the larger concentration of defects prevents the formation of the regular pattern evident in [27]. Note also that, in case the size of the particle becomes smaller than $\lambda$, the fluctuation of wavelength $\lambda$ can no longer be developed, in which case the solid solution is stabilized. This is actually in agreement with the recent results from Ref. [20], according to which solid solution is stabilized in particles of size $d = 40$ nm. We shall return to the nano-structured particles later in Section 5.

The existence of FP/LFP interfaces parallel to the ($bc$)-plane are clearly evident during the lithiation/delithiation process, as in Ref. [27], which suggests that it is a general feature of these materials, clearly linked to the cooperative motion of Li-atoms along $b$-channels. The situation, however, is more complex than expected. In particular, the strong dislocation strain fields in the ($ac$)-planes generate dislocations along other directions so that the size of the cross-section of LFP domains in the ($ac$)-planes remains finite upon delithiation, impeding the "stripe" geometry resulting from a motion of phase boundaries (unlimited along the $c$-direction) along the $a$-direction to develop like in Ref. [27]. These dislocations, however, are not accompanied by a geometric disorder beyond the

atomic length scale in their vicinity, so that the extraction/insertion process in our sample should not propagate through the diffusion associated with a concentration gradient that might exist in a disordered region. Instead, phase boundary motions and nucleation phenomena govern the dynamics. They have been considered in the most recent models [59], but not in the models that are based on the calculation of diffusion coefficients. Of course, the concept of "*apparent*" diffusion sometimes used to account for experimental data is a useful concept to characterize the kinetics, but the origin of lithium insertion/extraction process is not expected to be diffusive in nature at the atomic scale. It is due to a cooperative motion of Li ions in *b*-channels associated with a motion of dislocations and phase boundaries, the nucleation mechanism being responsible for the efficiency of charging LFP at high potential [60]. The cooperative motion of Li is the source of the ordering of domains, which has been observed in [27] in the form of ordered domains of FP spaced between the parent LFP domains. This ordering is not what is observed in our work, as we have quite a different picture of domains with finite cross-section in the (*ac*) plane. We have illustrated one particular LFP domain in Fig. 6, but actually, similar domains were found in many regions, at a density which is in agreement with the overall composition $x = 0.5$ of the sample. The reason for the appearance of such domains is presumably the smaller size of the crystallites, and more defects that reduce the coherence length of the XRD (smaller than the size of the particles evidenced on the SEM images in particular), thus preventing the formation of the coherent structure shown [27]. We then believe that the difference between the geometries of the domains observed for different samples is simply due to a difference in the concentration of defects. In particular, our results can be explained with the same mechanism of extraction/insertion of lithium described in Refs. [27,29], namely a collective motion of Li ions along the *b*-channels that generate strain and stress fields evidenced by the structural properties of the interfaces.

## 5. Discussion

We have shown that the formation of domains of different shapes, depending on the way the samples have been synthesized, can be understood in the framework of the standard models of the separation in two non-miscible phases, like the spinodal decomposition. Note that the model is a thermodynamic one, which implies that it holds true in the limit of an infinite size of the particles. In practice, it means sizes larger than the modulation parameter $\lambda$. For particles sizes $d$ of the order of $\lambda$, the modulation has not enough space to grow, impeding the de-mixing. This is actually consistent with the observation of the solid solution in particles 40 nm sized [20]. This result is at odds with the domino-cascade model, according to which the particles should be either in the LFP or in the FP composition. Two basic differences should be pointed out at this step between our model and the domino-cascade model: (a) in the limit $d \to \infty$, the domino-cascade model would require an interface moving at infinite speed to extract or insert all the $Li^+$ ions. (b) The domino-cascade model is not a model describing the system at equilibrium. Thermodynamic equilibrium between particles would require a physical contact under the form of a two-dimensional interface between them. However, there is no physical contact between the particles at all, since they are separated by about 7 nm of carbon (twice the thickness of the carbon layer). Therefore, at each step of the lithium/delithiation process in the domino-cascade model, each particle would be out of equilibrium, since none of them would have the desired concentration $x$ in lithium. On the other hand, according to our model, in the same limit $d \to \infty$, the picture is that of an infinite number of interfaces moving altogether at finite speed to adjust the proportion $x$ of Li-rich versus Li-poor domains to the desired concentration, so that equilibrium is reached inside each particle between the two phases. The limit $d \to \infty$ is thus, in our case, the thermodynamic limit. Note that the plateau in Fig. 8 supposes an equilibrium between the two phases inside the particles, as we have seen in the previous section, so that this feature of the electrochemical properties is consistent with our model, but not with the domino-cascade model.

The efficiency of the lithium insertion/extraction process in our view comes from the fact that the modulated structure percolates, i.e. it is possible to connect any lattice site inside the particle to the surface of the particle by jumps on nearest neighboring sites inside the same (Li-rich or Li-poor) region. This geometric property is evident from the simple fact that the model is thermodynamic in essence, i.e. the modulated structure is formed in the whole particle to create domains that percolate throughout the particle. This is trivial in case the pattern is that of stripes. In the case experienced in the present work, the connection is mediated by the third dimension, whether the interfaces are parallel to the (*bc*) plane [27] or oriented differently [29]. The percolation allows for the collective and coherent motion of the lithium ions inside the whole particle to and from the surface, instead of the uncorrelated diffusion of each Li ion that would be much less efficient. Actually, in our oversimplified model, the modulation length should depend on the temperature only, at least for particles of large enough size so that the elastic constants remain the same as those of the bulk material. If $d_a$ and $d_b$ are the "width" of the A and B domains, the growth of one phase, say A, with respect to the other one B should be performed by increasing $d_a$ and decreasing $d_b$, the period $d_a + d_b = \lambda$ remaining constant. This behavior could not be checked yet in the lithiation/delithiation process of LFP, but it has been observed in the topological hysteresis of the stripe domain structure of magnetic bubbles [61], a more favorable case since $d_a$, $d_b$ in the latter case depend not only on the temperature, but also on the magnetic field $H$ applied to the material, which can be easily varied.

Note that we have been most concerned in the model with the formation of domains, and their evolution when chemical or electrochemical energy is provided to the particles. But self-organized structures can also reach equilibrium: once formed, the patterns are stable and do not require additional energy. This is indeed what is observed here, since the TEM images in the present work or in prior works do not change with time. Indeed, there are a great variety of physical and chemical systems that exhibit such modulated patterns at equilibrium. We may cite magnetic bubbles as above-mentioned, in which case the interfaces are Bloch walls, or superconducting materials, block co-polymers, phospholipids, ferrofluids, and liquid crystals (see [62] and references therein). We can also learn from these studies that dislocations facilitate the coarsening of the magnetic-stripe domain patterns [63]. In the same way, the dislocations we have observed in the TEM image may also play this role in our case. In most cases encountered in nature, however, the patterns are obtained with various morphologies, depending only on the preparation conditions [64,65]. These conditions are also important in our case, since the patterns are different for different samples investigated. In addition, however, the geometry of the interface, dictated by the topology of the crystal lattice (flat interface moving parallel to itself), also plays an important role in the layout of the pattern. This is the main feature of the lithiation/delithiation process in LFP.

Our model presented in this work is expected to be valid in a finite range of particles sizes. The particles should be small enough so that the $LiFePO_4$ and $FePO_4$ domains should percolate throughout the structure. In practice, this will probably mean submicron-sized particles [66]. More importantly, we have pointed out that the particles should also have diameter $d$ at least comparable to the characteristic length $\lambda \approx 50$ nm. This, however, is only the order of magnitude. $\lambda$ is expected to vary with $d$, since the elastic constants vary with $d$ at the nanoscale, and so will the

stress/stain fields inside the particles. From an experimental point of view, we have argued that particles with $d = 45$ nm are still biphased when the disorder inside the surface layer is minimized [67], so that the critical size $d_c$ for the vanishing of the miscibility gap should be significantly smaller than expected from prior studies [18]. This conclusion [67,68] is in agreement with recent calculations of the surface energy [69]. In addition, we have argued that the larger range of Li-concentrations where the solid solution observed sometimes for particles of similar sizes is an artifact due to the passivation layer, when it is strongly disordered. This feature provides evidence that the disorder/defects stabilize the solid solution. Therefore, the question whether the solid solution observed in particles of size $d = 40$ nm that contain many defects is an intrinsic property of particles of such small size, or the consequence of the defects, or is observed only inside the passivation layer where it exists, is an open question. Therefore, the lower size limit for the validity of our model of morphology of the domains in the present work is not yet fully determined experimentally yet, but it should extend at least down to 45 nm. For smaller sizes, the phase diagram of $LiFePO_4/FePO_4$ should be revisited in view of our results [67,68] according to which, the size effect on the intrinsic properties should be distinguished from the effect of the disorder associated in particular with the passivation layer. Note that, according to our model, the disorder will oppose the formation of the modulated structure and the propagation of the interface, so that again the single phase will be stabilized. The increasing effect of the disorder upon decreasing the size of the particle below 50 nm, and the concomitant stabilization of the solid solution by the disorder are thus in agreement with our model.

## 6. Concluding remarks

Our results invalidate the core–shell model, since we find that both phases exist in the surface layer. They also invalidate the new "domino-cascade" model proposed in Ref. [32], according to which each particle would be single-phased, either FP or LFP. This model is intended to explain the fact that the lattice coherence length is the same before and after delithiation. We did find that this coherence length does not depend on the degree of delithiation, but still we do have the co-existence of the two phases inside the particles. The reason is that the coherence length of the lattice can be considered as the average distance between crystal defects, and since these crystal defects are also nucleation centres for the formation of LFP or FP domains, the size of these domains is also about the same as the coherence length, which is then unaffected in the lithiation/delithiation process. Therefore, this property does not imply, as it was postulated in Ref. [32], that the particles are single-phased, and indeed, they are not. This invalidation of the domino-cascade model also exempts us from the unanswered questions to find out how one particle chooses to be in one phase while another one remains in the other phase without violating the causality principle. Since the basic idea of this model is that the interface moves so fast that the particles are almost instantaneously lithiated or delithiated, the dispersion in size of the particles is of no importance. Another question that the domino-cascade model should have raised is the coherence with the electrochemical properties, since both the existence of the plateau in Fig. 8, and the value of its potential at 3.4 V are understood only if there is an equilibrium between Li-rich and Li-poor phases implying the existence of an interface inside the particles. The domino-cascade model would thus violate also the Gibbs phase rule.

The first result of the present work is then the confirmation of the models of lithium extraction/insertion of Refs. [27,29] that the present work complement; they are compatible, not only with the analysis of the structural properties, but also with the electrochemical properties, to the detriment of other models [32].

The difference in the amount of defects and in the geometry of the domains does not have any impact on the electrochemical performance of the product as a cathode element, at least for particles of size anywhere in the range $45 < d < 400$ nm that we have investigated so far, in this work and in prior works. This outstanding result can be understood as an "extended recovery" quite similar to the situation met in super-plastic aluminum alloys, and indeed, we have found that the topology of the LFP/FP interface satisfies the conditions required for super-plasticity. Attention should now be focused on the phase diagram of LFP for particle size $d < 40$ nm, following the same procedure used to obtain particles of size $d \approx 45$ nm without any defect or any impurity, and with minimized disorder in the passivation layer [67,68] to determine the limit of validity of our model, with stabilization of the solid solution as the ground state at room temperature.

## Acknowledgment

The authors wish to thank Dr. Michel Armand from CNRS (University of Amiens) for the careful reading and helpful discussions of the manuscript.

## References

[1] A.K. Padhi, K.S. Nanjundaswamy, J.B. Goodenough, J. Electochem. Soc. 144 (1997) 1188.
[2] N. Ravet, Y. Chouinard, J.F. Magnan, S. Besner, M. Gauthier, M. Armand, J. Power Sources 97 (2001) 503.
[3] A. Yamada, S.C. Chung, K. Hinokuma, J. Electrochem. Soc. 148 (2001) A224.
[4] A. Ait-Salah, A. Mauger, K. Zaghib, J.B. Goodenough, N. Ravet, M. Gauthier, F. Gendron, C.M. Julien, J. Electrochem. Soc. 153 (2006) A1692.
[5] C.M. Julien, A. Mauger, A. Ait-Salah, M. Massot, F. Gendron, K. Zaghib, Ionics 13 (2007) 395.
[6] H. Huang, S.-C. Yin, L.F. Nazar, Electrochem. Solid State Lett. 4 (2001) A170.
[7] K. Zaghib, N. Ravet, M. Gauthier, F. Gendron, A. Mauger, J.B. Goodenough, C.M. Julien, J. Power Sources 163 (2006) 560.
[8] D. Morgan, A.V.D. Ven, G. Ceder, Electrochem. Solid State Lett. 7 (2004) A30.
[9] S.M. Islam, D.J. Driscoll, C.A.J. Fisher, P.R. Slater, Chem. Mater. 17 (2005) 5085.
[10] T. Maxisch, F. Zhou, G. Ceder, Phys. Rev. B 73 (2006) 10431.
[11] K. Zaghib, A. Mauger, J. Goodenough, F. Gendron, C.M. Julien, Chem. Mater. 19 (2007) 3740.
[12] C. Delacourt, P. Poizot, J.M. Tarascon, C. Masquelier, Nat. Mater. 1 (2002) 123.
[13] C. Delacourt, J. Rodriguez-Carjaval, B. Schmitt, J.M. Tarascon, C. Masquelier, Solid State Sci. 7 (2005) 1506.
[14] J.L. Dodd, R. Yazami, B. Fultz, Electrochem. Solid-State Lett. 9 (2006) A151.
[15] R. Stevens, J.L. Dodd, M.G. Kresch, R. Yazami, B. Fultz, B. Ellis, L.F. Nazar, J. Phys. Chem. B 101 (2006) 22732.
[16] G. Chen, X. Song, T.J. Richardson, J. Electrochem. Soc. 154 (2007) A627.
[17] T.J. Richardson, Third Annual Conference: LITHIUM MOBILE POWER 2007—Advances in Lithium Battery Technologies for Mobile Applications, San Diego, USA.
[18] A. Yamada, H. Koizumi, S. Nishimura, N. Sonoyama, R. Kanno, M. Yonemura, T. Nakamura, T. Kobayashi, Nat. Mater. 5 (2006) 354.
[19] N. Meetong, H. Huang, W.C. Carter, Y.M. Chiang, Electrochem, Solid State Lett. 10 (2007) A134.
[20] P. Gibot, M. Casas-Cabanas, L. Laffont, S. Levasseur, P. Carlach, S. Hamelet, J.-M. Tarascon, C. Masquelier, Nat. Mater. 7 (2008) 741.
[21] M.S. Whittingham, Y. Song, S. Lutta, P. Zavalij, N.A. Chernova, J. Mater. Chem. 15 (2005) 3362 (and references therein).
[22] S. Franger, C. Bourbon, F. Le Cras, J. Electrochem. Soc. 151 (2004) A1024.
[23] S.W. Song, R.P. Reade, R. Kostecki, K.A. Striebel, J. Electrochem. Soc. 153 (2006) A12.
[24] D.Y. Yu, C. Fietzek, W. Weydanz, K. Donoue, T. Inoue, H. Kurokawa, S. Fujitani, J. Electrochem. Soc. 154 (2007) A253.
[25] T. Nakamura, K. Sakumoto, S. Seki, Y. Kabayashi, M. Tabuchi, Y. Yamada, J. Electrochem. Soc. 154 (2007) A1118.
[26] A. Mauger, Phys. Rev. E 71 (2005) 11019.
[27] G. Chen, X. Song, T.J. Richardson, Electrochem. Solid-State Lett. 9 (2006) A295.
[28] V. Srinivasan, J. Newman, J. Electrochem. Soc. 151 (2004) 1517.
[29] L. Laffont, C. Delacourt, P. Gibot, M. Yue Wu, P. Kooyman, C. Masquelier, J.M. Tarascon, Chem. Mater. 18 (2006) 5520.
[30] A. Yamada, H. Koizumi, N. Sonoyama, R. Kanno, Electrochem. Solid State Lett. 8 (2005) A409.
[31] A.S. Andersson, J.O. Thomas, J. Power Sources 97 (2001) 498.
[32] C. Delmas, M. Maccario, L. Croguennec, F. Le Cras, F. Weill, Nat. Mater. 7 (2008) 665.
[33] K. Zaghib, M. Armand, HQ Internal Report, 1997; First PBFC, Jeju, Korea, 2003.

[34] S. Yang, P.Y. Zavalij, M.S. Whittingham, Electrochem. Commun. 3 (2001) 505.
[35] A. Ait-Saklah, J. Dodd, A. Mauger, R. Yazami, F. Gendron, C. Julien, Zeit. Anorg. Allg. Chem. 632 (2006) 1598.
[36] V.A. Streltsov, E.L. Belokoneva, V.G. Tsirelson, N.K. Hansen, Acta Crystallogr. B49 (1993) 147.
[37] N. Amdouni, K. Zaghib, F. Gendron, C.M. Julien, Ionics 12 (2006) 117.
[38] A. Ait-Salah, A. Mauger, C.M. Julien, F. Gendron, Mater. Sci. Eng. B 129 (2006) 232.
[39] C.A.J. Fisher, M.S. Islam, J. Mater. Chem. 18 (2008) 1209.
[40] R.D. Doherty, D.A. Hughes, F.J. Humphreys, J.J. Jonas, D.J. Jensen, M.E. Kassner, W.E. King, T.R. McNelleyh, H.J. McQueeni, A.D. Rollett, Mater. Sci. Eng. 219 (1997) A238.
[41] E.J. Nes, Mater. Sci. Eng. 13 (1978) A2052.
[42] S.J. Hales, T.R. Mc Nelley, H.J. Mc Queen, Metal Trans. 22 (1991) A1037.
[43] C.M. Julien, K. Zaghib, A. Mauger, M. Massot, A. Salah, M. Selmane, F. Gendron, J. Appl. Phys. 100 (2006) 63511.
[44] K. Zaghib, M. Dontigny, P. Charest, J.F. Labrecque, A. Guerfi, M. Kopec, A. Mauger, F. Gendron, C.M. Julien, J. Power Souces 185 (2008) 698.
[45] W. Paraguassu, P.T.C. Freire, V. Lemos, S.M. Lala, L.A. Montoro, J.M. Rosolen, J. Raman Spectrosc. 36 (2005) 213.
[46] C. Burba, R. Frech, J. Electrochem. Soc. 151 (2004) A1032.
[47] D.X. Gouveia, V. Lemos, J.A.C. de Paiva, A.G. Souza Filho, J. Mendes Filho, Phys. Rev. B72 (2005) 024105.
[48] N. Meethong, H.-Y.S. Huang, S.A. Speakman, W.C. Carter, Y.-M. Chiang, Adv. Funct. Mater. 17 (2007) 1115.
[49] A. Manthiram, J.B. Goodenough, J. Power Sources 26 (1989) 403.
[50] V.A. Streltsov, E.L. Belokoneva, V.G. Tsirelson, N. Hansen, Acta Cryst. B49 (1993) 147.
[51] D. Wang, X. Wu, Z. Wang, L. Chen, J. Power Sources 140 (2005) 125.
[52] A.P. Sutton, R.W. Balluffi, Interfaces in Crystalline Materials, Clarendon Press, Oxford, 1995.
[53] D.Y. Yoon, Y.K. Cho, J. Mater. Sci. 40 (2005) 861.
[54] B.B. Straumal, S.A. Polyakov, E. Bischoff, W. Gust, E.J. Mittemeijer, Interf. Sci. 9 (2001) 287.
[55] S.B. Lee, W. Sigle, M. Rühle, Acta Mater. 51 (2003) 4583.
[56] B.B. Straumal, S.A. Polyakov, E.J. Mittemeijer, Acta Mater. 54 (2006) 167.
[57] D.M. Kirch, B. Zhao, D.A. Molodov, G. Gottstein, Scripta Mater. 56 (2007) 939.
[58] R.A.L. Jones, Soft Condensed Matter, Oxford University press, 2007.
[59] G.K. Singh, G. Ceder, M.Z. Bazant, Electrochem. Acta 53 (2008) 7599–7613.
[60] A. Yamada, M. Yonemura, Y. Takei, N. Sonoyama, R. Kanno, Electrochem. Solid-State Lett. 8 (2005) A55.
[61] P. Molho, J. Gouerzgh, J.C.S. Levy, J.L. Porteseil, J. Mag. Mag. Mater. 54–57 (1986) 857.
[62] M. Seul, D. Andelman, Science 267 (1995) 476.
[63] M. Seul, R. Wolfe, Phys. Rev. Lett. 68 (1992) 2460.
[64] N. Bowden, S. Britain, A.G. Evans, J.W. Hutchinson, G.M. Whitesides, Nature 393 (1998).
[65] J. Genzer, J. Groenewold, Soft. Mater. 2 (2006) 310.
[66] T. Richardson, Pacific Rim Meeting on Electrochemical and Solid-State Science PRIME 2008, Honolulu, HI, ext. Abstract #593.
[67] K. Zaghib, A. Mauger, F. Gendron, C.M. Julien, Chem. Mater. 20 (2008) 462.
[68] K. Zaghib, A. Mauger, F. Gendron, C. M. Julien, Pacific Rim Meeting on Electrochemical and Solid-State Science PRIME 2008, Honolulu, HI, ext. Abstract #581.
[69] G. Ceder, L. Wang, A. Belcher, Y. Lee, K. Kang, Pacific Rim Meeting on Electrochemical and Solid-State Science PRIME 2008, Honolulu, HI, ext. Abstract #627.